

UDC 621.372.22

# Lumped-Distributed Low-Pass Filters Based on Bragg Hybridization Effect

*Nelin E. A.*

National Technical University of Ukraine «Igor Sikorsky Kyiv Polytechnic Institute», Kyiv, Ukraine

E-mail: [ye.nelin@gmail.com](mailto:ye.nelin@gmail.com)

This paper proposes and investigates a novel approach to the design of low-pass filters (LPFs) based on the Bragg hybridization (BH) effect implemented in a lumped-distributed configuration. The scientific novelty lies in retaining the structural periodicity, contrary to traditional synthesis methods that introduce periodicity disruption to minimize ripple. It is demonstrated that restoring the coherence of Bragg synchronism and coupling it with the local resonance of low- $Q$  elements resolves the trade-off between stopband suppression and impedance matching. The results show that the synchronization of local and Bragg resonances ensures a continuous stopband, effectively eliminating spurious ripples within the rejection band. A collective transmission zero is formed at the Bragg frequency due to the coherent interaction of the resonators, shifting the first parasitic response to twice the Bragg frequency. For the developed LPF based on four  $\pi$ -sections, the calculated fractional rejection bandwidth relative to the cut-off frequency is 570% at the  $-60$  dB level and 378% at  $-100$  dB, with a passband ripple of 0.2 dB. The lengths of the considered LPFs are approximately twice as small as those of conventional elliptic filters. Utilizing the low- $Q$  BH mode significantly reduces sensitivity to dissipative losses and manufacturing tolerances compared to high-order elliptic filters. Given the use of normalized parameters, the proposed structures serve as generalized templates for the rapid design of miniature LPFs. The findings have direct practical implications for high-performance signal processing systems.

*Keywords:* Bragg hybridization; low-pass filter (LPF); lumped-distributed structures; coherent synchronism; collective transmission zero; stopband enhancement

DOI: [10.64915/RADAP.2026.104.74-80](https://doi.org/10.64915/RADAP.2026.104.74-80)

## Introduction

Microwave low-pass filters (LPFs) are widely used in various radio-electronic systems to suppress unwanted harmonics and spurious signals. The primary trends in the development of such devices include improving frequency response (FR) — specifically increasing the shape factor (SF) and expanding the stopband — as well as miniaturization and the implementation of Integrated Passive Device (IPD) technology [1–8]. These directions are driven by the stringent requirements of modern communication, radar, and electronic warfare systems.

Traditional approaches to LPF design are limited by the capabilities of classical synthesis methods, which do not allow for the simultaneous achievement of an ultra-wide stopband with high suppression levels and significant device miniaturization. This work demonstrates that this challenge can be addressed by employing the Bragg hybridization (BH) mechanism.

Bragg hybridization is a wave phenomenon in periodic structures characterized by the synergetic interaction between the local resonances of its elements and the Bragg reflection from the periodic medium.

The key condition for BH — the alignment of the local resonance frequency with the Bragg frequency — ensures the formation of a wide and deep bandgap (stopband), which is a fundamentally new property compared to the separate manifestations of these phenomena. Although BH effects are actively studied in the physics of metamaterials (primarily acoustic) [9–11], there is a lack of information in the literature regarding their application in microwave device engineering. It should be noted that the physical nature of the anomalously wide rejection band observed in two of the resonators discussed in [12] can be explained specifically by the BH mechanism, which has not been previously addressed as a separate subject of study.

The implementation of BH in this work is distinguished by the use of low- $Q$  resonators with a series resonance characteristic. Unlike classical BH metamaterial models based on high- $Q$  (often idealized infinite- $Q$ ) parallel resonance elements, the proposed approach ensures a transition from narrow-band hybridization to wide-band interaction that is robust against dissipative losses and manufacturing tolerances. This BH regime enables a wide stopband, which is critical for modern wideband communication systems.

The aim of this work is to significantly expand the stopband and achieve miniaturization of a microwave LPF by employing a design based on BH. For modeling purposes, the transmission line (TL) model, which is applicable to various types of microwave filters, is utilized. Characteristic impedances and input admittances are normalized to the corresponding parameters of the TL.

## 1 Conventional LPF Based on a Bragg Reflector

Bragg reflectors are widely used in optics. These reflectors have also found applications in microwave engineering. This is due to the reflector's ability to create a clear bandgap (stopband). A conventional microwave LPF in the form of a periodic structure formed by alternating TL sections (Fig. 1) acts as a Bragg reflector within the stopband.

Figure 1a shows the schematic of a lumped LPF of five order. Figure 1b illustrates the signal conductor for the microstrip implementation of such an LPF. Capacitors and inductors are implemented as quasi-lumped elements using wide and narrow sections with low and high characteristic impedances, respectively. This LPF is an example of a periodic structure.

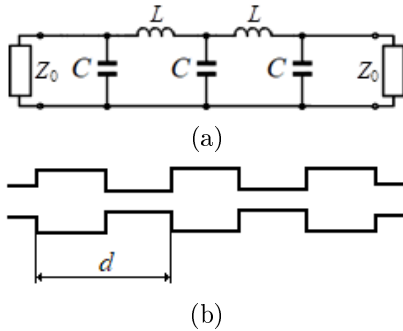


Fig. 1. Lumped-element LPF schematic:  $C$  and  $L$  are capacitors and inductors,  $Z_0$  is the characteristic impedance of the TL (a); signal conductor of the Bragg-type microstrip LPF:  $d$  is the period (b)

The transmission characteristic of a periodic structure consists of alternating passbands and bandgaps, which correspond to the passbands and stopbands of the FR. The first passband and the first bandgap constitute the passband and stopband of the Bragg LPF. The transmission characteristic of a model infinite periodic structure have ideal levels of 1 and 0 in the passbands and bandgaps, respectively. In the transmission characteristic of a real finite periodic structure, ripples occur in the passband, the transition to the bandgap has a finite slope, and the level in the bandgap gradually decreases to a minimum, which corresponds to the maximum reflection coefficient.

The Bragg condition

$$d = \lambda/2, \quad (1)$$

where  $\lambda$  is wavelength, corresponds to the maximum reflection coefficient in the first bandgap (LPF stopband).

Such an LPF is characterized by a simple structure and a wide stopband, but it also has significant drawbacks: 1) a high ripple level in the passband; 2) the reflection efficiency is substantially limited by the achievable characteristic impedance values, which, in turn, limits the suppression level in the stopband.

To reduce the ripple level, apodization of the LPF is required by varying the element widths and characteristic impedance values. This leads to increased structural complexity, degraded suppression levels, and a significant narrowing of the stopband. The nearest spurious response appears as early as the Bragg frequency, which serves as the center frequency of the stopband in the absence of apodization. The latter drawback is characteristic of any filters based on TL sections, since the lack of periodicity leads to the appearance of the nearest spurious response exactly at the half-wavelength (Bragg) frequency of the longest TL section.

The low- $Q$  BH mode proposed and implemented in this work, as demonstrated below, allows for overcoming the aforementioned fundamental drawbacks of the conventional Bragg FR formation mode, not only preserving but significantly enhancing its advantages.

## 2 $\pi$ -type lumped-distributed LPF section

Figure 2 illustrates a subwavelength resonator similar to those proposed in [12]. Its principle of operation is analogous to an optical Fabry-Pérot resonator, consisting of a resonant cavity and reflectors at its boundaries. The microwave resonator cavity is implemented as a through TL section (hereinafter referred to as the series section), while the reflectors are implemented as lumped-distributed (hybrid) series resonant circuits. The circuit capacitance is lumped, where as the inductance is quasi-lumped, realized as a short TL section (hereinafter referred to as the shunt section). The resonant frequency of the circuit  $f_r$  coincides with the quarter-wavelength frequency  $f_{\lambda/4}$  of the series section:

$$f_r = f_{\lambda/4}. \quad (2)$$

The resonant frequency of the resonator is significantly lower than the traditional half-wavelength frequency of the section due to the phase shift during reflection. The reflectors form a wide rejection band at the frequency  $f_{\lambda/4}$ . The resonator is capacitively coupled to external circuits. A set of such resonators with mutual capacitive coupling forms a miniature band-pass filter. The FR of the filter exhibits a high SF and a wide high-frequency deep stopband.

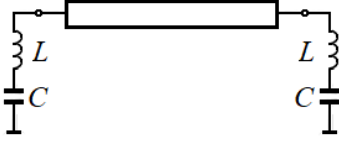


Fig. 2. Lumped-distributed microwave resonator

In the low-frequency range, with direct coupling to external circuits, the circuit shown in Fig. 2 acts as a  $\pi$ -type LPF cell. The series TL section forms a quasi-lumped inductive element, while the circuits serve as shunt elements. Such a cell exhibits a quasi-elliptic FR, characterized by a high SF and the presence of a transmission zero (rejection pole) in the stopband.

### 3 Comparison of $\pi$ -type cell characteristics

In order to suppress the nearest spurious resonance caused by the half-wavelength resonance of the hybrid cell's series TL section, the condition for the circuit's resonant frequency, in contrast to (2), must be satisfied as follows:

$$f_r = f_{\lambda/2}, \quad (3)$$

where  $f_{\lambda/2}$  is the half-wavelength frequency of the section.

Condition (3) corresponds to the BH regime (1), where the frequency  $f_{\lambda/2}$  serves as the Bragg frequency. For structures with a small number of elements (2–3 elements), specifically for subwavelength resonators, the maximum rejection band corresponds to the quarter-wavelength condition (2). This is attributed to the rapid wave attenuation in low- $Q$  elements, causing the dominant mechanism to be the destructive interference of waves reflected once from the nearest elements, while the collective BH effect is not fully manifested.

To determine the lumped capacitance, we utilize the characteristic impedance of an open-circuited stub. The stub has the same capacitance at  $f = 0$  and the same series resonance frequency as the series resonant circuit. This approach enables calculations in normalized frequencies  $F = f/f_{\lambda/2}$  (where  $f$  is the current frequency), which eliminates the dependence on the absolute frequency value. The stub capacitance is given by:

$$C = \frac{1}{4Z_0 z_C f_{\lambda/2}},$$

where  $z_C$  is the normalized characteristic impedance of the stub. For example, if  $Z_0 = 50\Omega$ ,  $z_C = 0.5$  and  $f_{\lambda/2} = 10$  GHz, then  $C = 1$  pF.

Let us compare, under identical conditions, the FR of the hybrid  $\pi$ -cell (cell 1) and the  $\pi$ -cell with resonant shunt elements in the form of quarter-wavelength open-circuited stubs (cell 2). The capacitances (for cell 2 — at  $f = 0$ ), as well as the resonance frequencies of the

stubs and circuits, are identical for both cells. Figs. 3a and b illustrate these cells in the microstrip version.

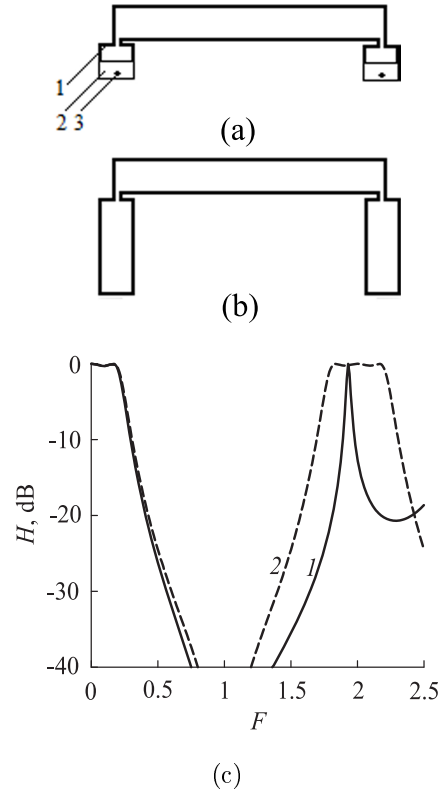


Fig. 3. Hybrid  $\pi$ -cell 1 (a), 1 – quasi-lumped inductance (short TL section), 2 – lumped miniature capacitor, 3 – grounding via;  $\pi$ -cell 2 (b); FRs of cells 1 and 2 (1 and 2, respectively) (c)

Figure 3c shows the FRs of cells 1 and 2. These responses, as well as those presented in Figs. 4–6, are calculated without losses. The impact of losses is discussed in Section 4. Parameters:  $z_C = 0.5$ ,  $z = 2$ ,  $z_1 = 0.62$ ,  $l_1 = 0.04$ , where  $z$  and  $z_1$  are the characteristic impedances of the series and shunt sections, respectively,  $l_1$  is the length of the shunt section normalized to the wavelength at the frequency  $f_{\lambda/2}$ . The  $Q$ -factor of the circuits in cell 1 is 0.4.

The ripple level of the FR for both cells is 0.3 dB. The cutoff frequencies for cells 1 and 2 at the  $-3$  dB level are  $F_c = 0.229$  and  $0.236$ , respectively. Cell 1 exhibits higher shunt capability; therefore, its FR has a steeper SF, a wider rejection band, and a lower cutoff frequency. Cell 2 features a wide spurious response caused by the parallel resonance of the stubs. The transverse dimension of cell 1 is substantially smaller than that of cell 2, because the quasi-lumped inductance is implemented by a much shorter section than the quarter-wavelength stub of cell 2, and the capacitor is a miniature thin-film type.

## 4 Filters based on hybrid $\pi$ -type cells

Let us consider the FRs of LPFs based on hybrid  $\pi$ -type cells. The conventional design methodology consists of determining the parameters of each series and shunt element according to the specified FR requirements. The resonance frequencies of the shunt elements are distributed within the stopband to ensure the required positioning of the transmission zeros.

The design of LPFs based on the BH effect has distinct differences. All series elements of the cells are identical, and the local resonant circuits are tuned to a single frequency according to condition (3). The internal circuits are shared between adjacent cells, and the element parameter values are chosen to be identical relative to the symmetry axis of the filter structure. The periodicity of the LPF structure, combined with the single-frequency tuning, ensures the emergence of the BH effect.

Filter FR parameters:  $F_c = 0.23$ , passband ripple level 0.2–0.3 dB. Design parameters are presented in Table 1, where No is the filter number corresponding to the number of cells (LPF 1 corresponds to the previously discussed cell 1). Circuit parameters:  $z_{C1}$ – $z_{C3}$  are the characteristic impedances of the capacitances  $C_1$ – $C_3$ , while  $z_1$ – $z_3$ ,  $l_1$ – $l_3$  are the corresponding parameters of the inductances  $L_1$ – $L_3$  (numbered from the edges toward the center of the LPF, Fig. 4a),  $l$  is the total length of the LPF normalized to the wavelength at the cutoff frequency  $\lambda_c$ .

Figure 4a shows the schematic of LPF 4. Figure 4b illustrates the increase in the SF and the expansion of the stopband as the number of cells increases.

The stopband is a continuous rejection band resulting from BH. Within the stopband, the FRs clearly demonstrate the growing influence of the BH effect. The spurious response is caused by the coupled second resonances of the cells' series sections. The center frequency of this response is 2.0, which is 8.7 times higher than the cutoff frequency. The lengths of LPFs 1–4 range from 0.12 to  $0.46 \lambda_c$ . The stopband of LPF 4 relative to the Bragg frequency (1.0) at the –60 and –100 dB levels is 131% and 87%, respectively, and relative to the cutoff frequency, it is 570% and 378%.

Table 1 Design parameters of LPFs 1–4

No	$z$	$z_{C1}$	$z_{C2}$	$z_{C3}$	$z_1$	$l_1$	$z_2$	$l_2$	$z_3$	$l_3$	$l$
1	2.00	0.50	-	-	0.62	0.04	-	-	-	-	0.115
2	2.00	0.55	0.33	-	0.68	0.04	0.55	0.03	-	-	0.230
3	2.05	0.64	0.34	-	1.07	0.03	0.56	0.03	-	-	0.345
4	2.10	0.90	0.34	0.36	1.12	0.04	0.60	0.03	0.57	0.03	0.460

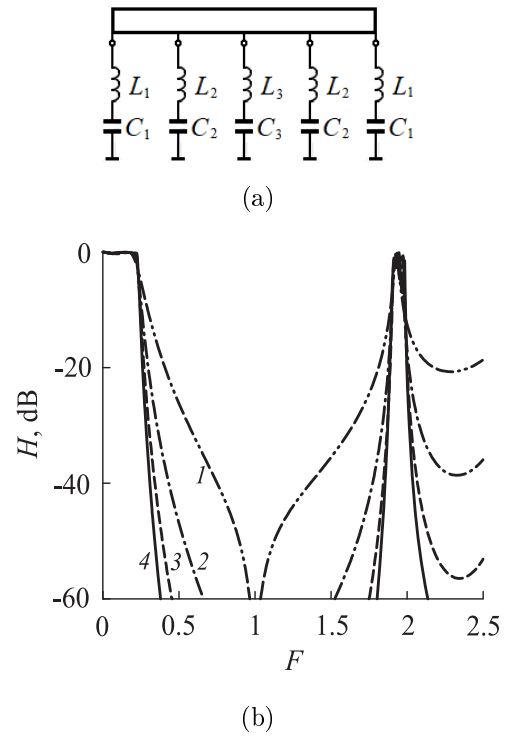


Fig. 4. Schematic of LPF 4 (a); FRs of LPFs 1–4 (1–4, respectively) (b)

The BH effect is quantitatively equivalent to a significant mismatch of the characteristic impedances in a periodic structure. This is illustrated in Fig. 5, which shows the FRs of LPF 4 and a conventional Bragg reflector formed by alternating quarter-wavelength TL sections with an impedance ratio of  $z/1$ . For the same cutoff frequency and number of periods, the value of  $z$  is 25.7, indicating the remarkably high efficiency of BH. Such a value lies far beyond the limits of practical feasibility.

At the Bragg frequency, conventional Bragg reflection achieves only a finite minimum of the transmission coefficient, which is –107 dB, whereas the BH mode provides rejection with a wide stopband.

It should be noted that the ripple level of a conventional Bragg reflector is 13 dB. The BH mechanism provides effective self-matching within the passband. Unlike traditional periodic structures with high impedance contrast, BH forms an input impedance frequency dependence such that only weak apodization of the circuits'  $Q$ -factors is sufficient to achieve a ripple level of 0.2–0.3 dB.

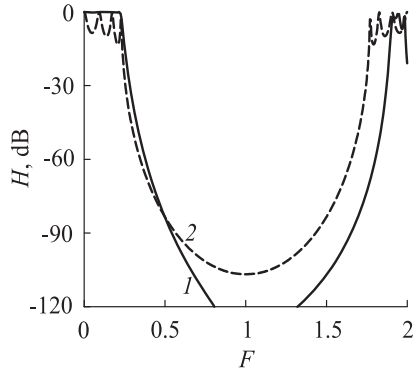


Fig. 5. Frequency responses of LPF 4 and a Bragg reflector (1 and 2, respectively)

The stopband of conventional LPFs is formed through complex amplitude-phase compensatory interference of partial incident waves. Such interference is sensitive to distortions caused by losses and manufacturing tolerances, especially at high suppression levels. The stopband of the proposed LPFs is formed by simple in-phase interference of reflected waves, which is robust against the aforementioned distortions.

A detailed comparative analysis of the effects of losses and manufacturing tolerances on the FR of the proposed LPFs is beyond the scope of this paper. To evaluate the impact of losses, the FR of microstrip LPF 4 was calculated in the 0–10 GHz frequency range ( $f_{\lambda/2} = 5$  GHz), implemented on a Rogers RO 3010 substrate with a thickness of 1.27 mm, considering typical capacitor losses. As expected, the losses result in some rounding of the FR in the passband. In the stopband, the lossy FR coincides with the lossless one, except for a rise near the Bragg frequency from a minimum level of  $-141$  dB to  $-112$  dB exactly at the Bragg frequency.

The use of normalized frequencies allows the considered LPFs to be used as templates for designing other LPFs. The normalized cutoff frequency  $F_c$  of the template serves as the reference for the calculation. From this frequency and the given actual cutoff frequency  $f_c$ , the half-wavelength frequency  $f_{\lambda/2}$  is determined:

$$f_{\lambda/2} = \frac{f_c}{F_c}. \quad (4)$$

Based on the obtained  $f_{\lambda/2}$  value and the TL parameters of a specific implementation, the unnormalized values of the design parameters are calculated. In the next stage, these values are refined by three-dimensional modeling.

## 5 Shape factor of LPF frequency responses

Let us consider the dependence of the SF on the filter order. The SF is defined at the  $-3$  and  $-40$  dB levels in dB/octave and compared with the asymptotic SF of Chebyshev or Butterworth filters.

The asymptotic SF is  $k_a = 6n$ , where  $n$  is the filter order. Table 2 presents the SF  $k$  and, for comparison, the asymptotic SF.

Table 2 Shape factor of LPFs 1–4

No	$n$	$k$	$k_a$
1	3	16	18
2	5	41	30
3	7	77	42
4	9	111	54

As the number of cells increases, the influence of the resonant nature of BH on the SF grows. The SF of LPF 4 is twice as high as the corresponding asymptotic value.

## 6 Increasing the shape factor and reducing element requirements

To increase the SF and reduce the requirements for the characteristic impedances and lengths of the TL sections, it is necessary to increase the normalized cutoff frequency. Fig. 6a and b show the FRs, and Table 3 presents the parameters of LPF 1\* and 4\*, which have the same number of cells as LPF 1 and 4, but with an increased  $F_c$  value. Here,  $F_s$  is the center frequency of the spurious response,  $s = F_s/F_c$ . The passband ripple level is 0.3 dB.

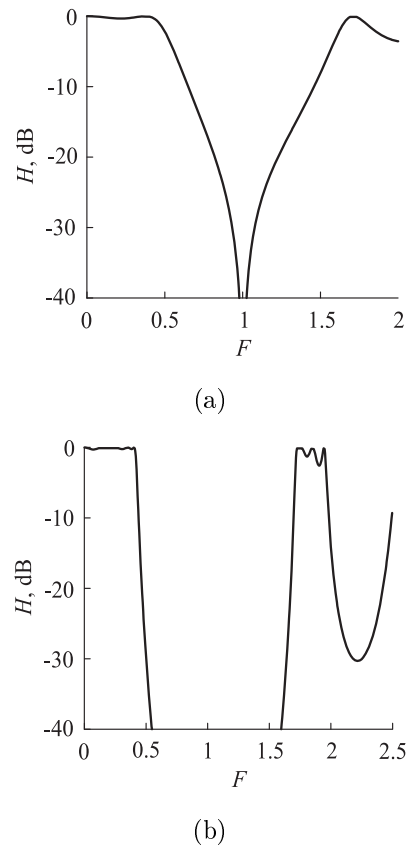


Fig. 6. Frequency responses of LPF 1\* (a) and 4\* (b)

Table 3 Parameters of LPF 1\* and 4\*

No	$z$	$z_{C1}$	$z_{C2}$	$z_{C3}$	$z_1$	$l_1$	$z_2$	$l_2$	$z_3$	$l_3$	$F_c$	$k$	$F_s$	$s$
1*	1.0	1.8	-	-	1.76	0.05	-	-	-	-	0.52	42	1.71	3.3
4*	1.2	1.5	0.9	0.8	1.45	0.05	0.9	0.03	0.8	0.03	0.42	126	1.84	4.4

Compared to LPF 1 and LPF 4, the normalized cutoff frequency of LPF 1\* and 4\* is approximately twice as high. For a given absolute cutoff frequency, according to (4), the frequency  $f_{\lambda/2}$  is twice as low. Consequently, the physical length of the short shunt TL sections increases. The SF of LPF 1\* has increased by 2.5 times and significantly exceeds the asymptotic value. The SF of LPF 4\* has increased by 15 dB/octave. In terms of asymptotic SF, LPF 4\*, which is of the 9th order, is equivalent to a conventional 21st-order filter. The maximum values and the range of characteristic impedances of the TL sections have decreased, simplifying the design and manufacturing requirements. The drawbacks of LPF 1\* and 4\* are the doubling of the device length and the narrowing of the stopband. Filters 1\* and 4\* can serve as alternative templates.

## 7 Discussion of the results

Conventionally, to minimize passband ripples, the periodicity of the structure is abandoned. A spurious response appears already at the half-wavelength frequency of the series TL sections (which is the Bragg frequency for the considered LPF), significantly narrowing the stopband. The lack of periodicity also results in a wide variety of element values. This imposes stringent design and manufacturing constraints and makes the characteristics sensitive to fabrication tolerances.

Maintaining periodicity in combination with the BH effect allows this contradiction to be resolved. The synchronization of local and Bragg resonances restores the coherence of the structure, which ensures a high suppression level and makes it possible to achieve passband ripples of 0.2–0.3 dB. To improve matching within the passband, only weak apodization of the shunt elements'  $Q$ -factors is required.

In the developed LPF based on four  $\pi$ -cells with a relative cutoff frequency of 0.23, the stopband at the –60 and –100 dB levels relative to the cutoff frequency is 570% and 378%, respectively. Unlike conventional filters, where ripples are observed in the stopband, they are absent in the BH-based LPF. This is explained by the formation of a collective transmission zero at the Bragg frequency (1.0) — a deep dip in the FR caused by the collective interaction of low- $Q$  resonant elements and the Bragg structure. This effect allows the spurious response to be shifted to a frequency of 2.0, more than doubling the stopband. In terms of periodic structures, the stopband corresponds to the bandgap,

where wave propagation is caused by tunneling with a characteristically very low transmission coefficient.

The lengths of the considered LPFs 1–4, which have orders from 3rd to 9th, range from 0.1 to 0.5  $\lambda_c$ , which is approximately twice as small as those of conventional elliptic filters.

Although theoretical models of elliptic filters may exhibit a higher SF, their practical implementation under strict suppression requirements is significantly limited by sensitivity to dissipative losses and manufacturing tolerances. In the proposed structure, high stability of characteristics is achieved, which allows maintaining deep and continuous stopband performance under real-world conditions.

Due to the use of normalized frequencies and equivalent characteristic impedances, the considered structures can serve as base templates for LPF design.

The application of modern miniature thin-film surface-mount capacitors allows for minimizing the transverse dimension of the LPF.

The transmission line model [13] used for performance calculation accounts for first-order effects and is universal for structures of various design implementations. This model is intuitive, unlike the much more complex three-dimensional model, which accounts for second-order effects and is intended for the analysis of specific types of structures.

The proposed solutions can be applied to various types of LPFs (microstrip, coaxial, etc.).

## Conclusions

1. Maintaining the periodicity of the LPF structure in combination with the BH effect allows for restoring the coherence of wave processes and overcoming the fundamental limitation of conventional synthesis methods regarding the interdependence between the suppression level and matching quality. The synchronization of local and Bragg resonances ensures a passband ripple level of 0.2–0.3 dB without disrupting the periodic nature of the device structure.

2. The formation of a collective transmission zero at the Bragg frequency, due to the collective interaction of low- $Q$  resonant elements, ensures the creation of a continuous bandgap without ripples. This allows for expanding the stopband of the developed LPF to 570% (at the –60 dB level) and shifting the spurious response to a frequency of 2.0.

3. The use of the low- $Q$  BH regime significantly reduces the sensitivity of filter characteristics to design and manufacturing tolerances, as well as to the

approximation of elements by TL sections. This makes the proposed structures more robust against fabrication deviations compared to high-order elliptic filters.

4. The practical significance of the work lies in the development of a generalized methodology for LPF design based on normalized parameters. This allows for the use of the proposed structures as templates for the rapid synthesis of miniature devices using a modern electronic component base.

## References

- [1] Luo Z., Yang L., Su T., Zhu X. and Gómez-García R. (2025). Single-Ended and Balanced Flat-Group-Delay RF Low-Pass Filters with Input-Quasi-Reflectionless Behavior for Digital-Communication Systems. *IEEE Trans. on MTT*, Vol. 73, Iss. 1, pp. 321–334. DOI: 10.1109/TMTT.2024.3430485.
- [2] Srivastava G. and Bhatt D. (2025). A High SFDR Wide-Bandwidth Third-Order Low-Pass Elliptic Filter in 180 nm CMOS Technology. *IEEE Microw. Wirel. Technol. Lett.*, Vol. 35, Iss. 11, pp. 1688–1691. DOI: 10.1109/LMWT.2025.3590977.
- [3] Tomar P. S. and Parihar M. S. (2024). The Design and Investigation of the Low-Pass Filter with High Selectivity and Ultra-Wide Stopband. *IETE Journal of Research*, Vol. 70, Iss. 3, pp. 2366–2371. DOI: 10.1080/03772063.2023.2185303.
- [4] Barou S., Zbitou J., Chahboun N. and Laaziz Y. (2025). Design and Simulation of a Semilumped Low-Pass Filter with Finite-Frequency Attenuation Poles for Wireless Power Transmission and Energy Harvesting. *Int. Conf. Funct. Mater. Renew. Energies*, Vol. 326, COFMER'05, DOI: 10.1051/epjconf/202532601007.
- [5] Santiago D., Laso M. A. G., Lopetegi T. and Arregui I. (2024). Robust and Flexible Design for Effective Low-Pass Filters Exploiting a Passband Replica. *IEEE Int. Microw. Filter Workshop (IMFW)*, pp. 35–38. DOI: 10.1109/IMFW59690.2024.10477129.
- [6] Yang L., Luo Z., Zhu X. and Gómez-García R. (2025). Two-Layer Balanced Low-Pass Filter with Multiple Transmission Zeros Using Microstrip-to-Microstrip Vertical Transitions. *IEEE MTT-S Int. Wireless Symp. (IWS)*, pp. 1–3. DOI: 10.1109/IWS65943.2025.11177693.
- [7] Liang R., Guo C., Shi G., Wang Z., Yang Q., Feng L., Li Y. and Zhang A. (2023). A W-Band Bandpass Filter with Dual Behavior Resonators Fabricated by Additive Manufacturing. *IEEE Microw. Wirel. Compon. Lett.*, Vol. 33, Iss. 11, pp. 1521–1524. DOI: 10.1109/lmwt.2023.3286574.
- [8] Li S., Jia R., Shi M. and Li S. (2025). A Compact Tunable Low-Pass Filter Based on Mixed Lumped-Distributed Circuit. *Int. Conf. Microw. Millimeter Wave Technol. (ICMMT)*, pp. 1–3. DOI: 10.1109/ICMMT65948.2025.11188601.
- [9] Chen S., Fang L., Liu J. and Wu S. (2024). An ultra-wideband plasmonic reflector based on local resonant bandgap and Bragg bandgap. *Optica Applicata*, Vol. LIV, Iss. 2, pp. 205–216. DOI: 10.37190/oa240207.
- [10] Cenedese M., Belloni E. and Braghin F. (2021). Interaction of Bragg scattering band gaps and local resonators in mono-coupled periodic structures. *J. Appl. Phys.*, Vol. 129, Iss. 12, 124501. DOI: 10.1063/5.0038438.
- [11] Croëgne C., Lee E. J. S. and Page J. H. (2022). Multimode propagation in phononic crystals with overlapping Bragg and hybridization effects. *Appl. Phys. Lett.*, Vol. 120, Iss. 3, 033104. DOI: 10.1063/5.0076628.
- [12] Nelin E. A. (2024). High-Selectivity Resonators Based on Transmission Line Sections. *IEEE 42st Int. Conf. Electron. Nanotechnol. (ELNANO)*, pp. 203–206. DOI: 10.1109/ELNANO63394.2024.10756869.
- [13] Awang Z. (2014). *Microwave Systems Design*. Springer Singapore, 313 p. DOI: 10.1007/978-981-4451-24-6.

## Зосереджено-розподілені фільтри низьких частот на основі ефекту брегівської гібридизації

Нелін Є. А.

У статті запропоновано та досліджено новий підхід до проектування фільтрів низьких частот (ФНЧ) на основі ефекту брегівської гібридизації (БГ), реалізованого у зосереджено-розподіленій конфігурації. Наукова новизна полягає у збереженні періодичності структури, на відміну від традиційних методів синтезу, де для мінімізації пульсацій використовують порушення періодичності. Доведено, що відновлення когерентності брегівського синхронізму та його поєднання з локальним резонансом низькодобротних елементів дає змогу розв'язати суперечність між рівнем подавлення у смузі подавлення та якістю узгодження імпедансів. Результати показують, що синхронізація локального та брегівського резонансів забезпечує суцільну смугу подавлення, ефективно усуваючи побічні пульсації в середині смуги режекції. Внаслідок когерентної взаємодії резонаторів на частоті Брега формується колективний нуль передачі, що змінює перший паразитний відгук на подвійну частоту Брега. Для розробленого ФНЧ на основі чотирьох  $\pi$ -ланок розрахункова відносна смуга режекції відносно частоти зрізу становить 570% за рівня  $-60$  дБ та 378% за рівня  $-100$  дБ при пульсаціях у смузі пропускання 0,2 дБ. Довжини розглянутих ФНЧ приблизно вдвічі менші, ніж у звичайних еліптичних фільтрів. Використання режиму низькодобротної БГ суттєво знижує чутливість до дисипативних втрат та виробничих допусків порівняно з еліптичними фільтрами високих порядків. Завдяки використанню нормованих параметрів запропоновані структури можуть слугувати узагальненими шаблонами для швидкого проектування мініатюрних ФНЧ. Отримані результати мають безпосереднє практичне значення для високоефективних систем обробки сигналів.

**Ключові слова:** брегівська гібридизація; фільтр низьких частот (ФНЧ); зосереджено-розподілені структури; когерентний синхронізм; колективний нуль передачі; розширення смуги подавлення